International Research Journal of Advanced Engineering and Science
ISSN (Online): 2455-9024

Development of a Thermal Model for the Prediction of Temperature Distribution at Arc Welding Surface

Adedeji. A. Kasali[1], Zokoro. S. Peter[1], Adedeji. T. Emmanuella[1]
[1]Department of Mechanical Engineering, Lagos State University, P.M.B.1087 Apapa, Lagos

Abstract**—***This study presents a thermal model for predicting temperature distribution during arc welding. A mathematical model was developed, and Rosenthal's 3D equation was applied to a semi-infinite workpiece to obtain an analytical solution. The welding simulation was then carried out using Abaqus software, and results were presented in the form of contour heat maps and graphs. The simulation results demonstrate the potential of the thermal model to accurately predict the temperature distribution during arc welding, and provide insights into the impact of different welding parameters on the temperature profiles. This information can be used to optimize welding processes and improve weld quality.*

Keywords**—** *Arc welding, Thermal model, Rosenthal's equation, Abaqus software, Temperature distribution, Weld quality.*

I. INTRODUCTION

Arc welding is a process that uses an electric arc to melt and fuse metal workpieces together. The arc is created between an electrode, which is usually made of a consumable metal wire, and the workpiece. As the arc heats the metal, it melts and fuses the workpieces together, forming a strong, permanent bond [1].

During welding, a significant amount of heat is generated at the welding surface. Accurate prediction of the temperature distribution is crucial for the development of high-quality welds. Over the years, several researchers have attempted to develop thermal models for predicting temperature distribution during arc welding. These models have considered various welding parameters, material properties, and boundary conditions to accurately predict the temperature distribution.

For instance, a model was developed for predicting temperature distribution during laser beam welding. The model considered the effects of laser power, welding speed, and material properties on the temperature distribution. It was validated using experimental data, and the results showed good agreement between the predicted and experimental values [2].

Similarly, a finite element model was developed for predicting temperature distribution during arc welding. They considered the effects of heat source, material properties, and boundary conditions on the temperature distribution. The model was validated using experimental data, and the results showed good agreement between the predicted and experimental values [3].

In another study, a three-dimensional (3D) thermal model was developed for gas tungsten arc welding (GTAW) and gas metal arc welding (GMAW). The model considered various parameters such as arc current, arc length, welding speed, and material properties to predict temperature distribution [4].

Despite the numerous studies on thermal modeling for predicting temperature distribution during welding, there is still a need for the development of accurate and efficient models. In this paper, we aim to develop a thermal model for predicting the temperature distribution during arc welding that considers various welding parameters and material properties.

II. METHODOLOGY

This study comprised mathematical modeling and computer modeling of arc welding in a bid to analyze the thermal behavior of. For the mathematical model, a three-dimensional rectangular coordinate system with a moving heat source was considered. For the computational modeling, two cuboidal bodies with equal dimensions of 100mm x 30mm x 2mm were joined together using the finite element-based commercial package of ABAQUS.

A. *Model Development for Arc Welding Process*

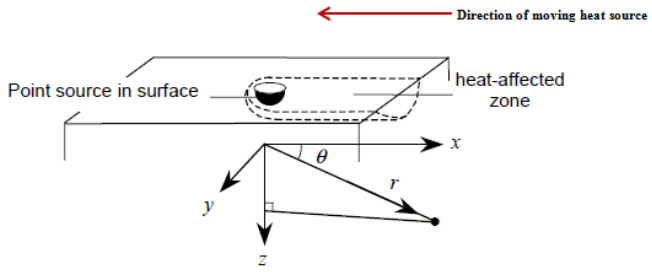

Fig. 1. Point source on the surface of the workpiece.

Fig. 1 shows a three-dimensional rectangular coordinate system with a moving heat source such as found in welding, surface hardening, laser cutting, milling process, continuous casting, and tribological applications. The moving heat source which is independent of time generates heat at a rate given by $\mathbf{Q_P}$. The heated zone starts from the right end of the bar and begins to move toward the left at a constant axial velocity of **u** along the slab.

The model is based on the following assumptions:

1. The tool material is isotropic and homogeneous;
2. The thermal properties of the material are independent of temperature;
3. No phase change occurs during the process;
4. Thermal boundary conditions are symmetrical across the manufacturing process centerline;
5. Heat transfer from the workpiece to the clamp is negligible.

Hence, the governing equation for the process is given by (1):

$$\frac{\delta T}{\delta t} = \alpha\left(\frac{\delta^2 T}{\delta x^2} + \frac{\delta^2 T}{\delta y^2} + \frac{\delta^2 T}{\delta z^2}\right) + Q_{work} \cdot \frac{A_r}{V} \qquad (1)$$

Where:

Adedeji. A. Kasali, Zokoro. S. Peter, and Adedeji. T. Emmanuella, "Development of a Thermal Model for the Prediction of Temperature Distribution at Arc Welding Surface," International Research Journal of Advanced Engineering and Science, Volume 8, Issue 2, pp. 165-171, 2023.

International Research Journal of Advanced Engineering and Science
ISSN (Online): 2455-9024

$\alpha = \frac{k}{\rho C_p}$;
A_r = arbitrarily selected area on the tool;
V = volume over which the heat generated on A_r is dissipated and the term;
Q_{work} = the rate of internal heat generation per unit volume of the slab/workpiece associated with the process and accounts for the boundary conditions.

Initial and Boundary Conditions

Initial condition:

$t = 0,\ T(x, y, z) = T_0$ (2)

Boundary Conditions

The heat flux boundary condition at the moving heat source-slab interface is:

$-k\frac{\delta T}{\delta z}|_{z=0} = \gamma Q_p,\ \ in\ the\ range\ \ R_p \le r \le\ R_p$ (3)

Where γ is a ratio according to which heat generated at the tool-workpiece interface is transported between the tool and the workpiece and is given as

$$\gamma = \frac{\sqrt{(k\rho C_p)_{slab/workpiece}}}{\sqrt{(k\rho C_p)_{slab/workpiece}} + \sqrt{(k\rho C_p)_{heat\ source/tool}}}$$

For the point-moving heat source under investigation, the term $Q_{slab/workpiece}$ has been taken to be invariant of *x* and *y*.

At the top surface beyond the shoulder, the boundary condition for heat exchange between the top surface of the workpiece and the surroundings involved convective and radiative boundary conditions.

$-k\frac{\delta T}{\delta z}|_{z=0} = h(T - T_a) + \sigma\varepsilon(T^4 - T_\infty^4)$ (4)

An effective heat transfer coefficient

$h_{eff} = h + \sigma\epsilon(T^3 + T_\infty T^2 + T_\infty^3)$ (5)

To linearize the convective and radiative effects at the boundary conditions in Eq. (4). Thus,

$-k\frac{\delta T}{\delta z}|_{z=0} = h(T - T_a), r \ge R_s$ (6)

The heat loss from the bottom surface is practically heated conduction from the workpiece and support base presents difficulty in modeling. To circumvent the problem and simplify the analysis, a high overall heat transfer coefficient was assumed. The heat loss was modeled approximately by using heat flux by convection

$-k\frac{\delta T}{\delta z}|_{z=0} = \beta_b(T - T_\infty)$ (7)

All other boundary conditions at ambient temperature

i.e. $T|_{y=-\infty} = T_\infty\ \ T|_{y=\infty} = T_\infty\ \ T|_{x=-\infty} = T_\infty\ T|_{x=\infty} = T_\infty$ (8)

As shown in Fig. 1, the welding heat source is moving with a constant velocity $\boldsymbol{u}$ in the opposite x-axis direction, a moving coordinate system "ς" is considered.

$\varsigma = \boldsymbol{x} - \boldsymbol{ut}$ (9)

ς is the radial distance of the heat source from a fixed position such that at any time $\boldsymbol{t}$. $\boldsymbol{ut}$ is the distance between the heat source and the origin of the fixed coordinate system (x, y, z) along the y-axis.

As $\boldsymbol{x}$ and ς are explicit functions of time $\boldsymbol{t}$, it is possible to write:

$\frac{\delta\varsigma}{\delta t} = -u$ (10)

We can also say that

$$\frac{\delta T}{\delta t} = \frac{\delta T}{\delta \varsigma}\cdot\frac{\delta \varsigma}{\delta t}$$

$\Rightarrow \frac{\delta T}{\delta t} = -u\frac{\delta T}{\delta \varsigma}$ (11)

Hence, (10) can now be rewritten as

$-u\frac{\delta T}{\delta \varsigma} = \alpha(\frac{\delta^2 T}{\delta \varsigma^2} + \frac{\delta^2 T}{\delta y^2} + \frac{\delta^2 T}{\delta z^2}) + Q_{work}\cdot\frac{A_r}{V}$

Let $Q_{work}\cdot\frac{A_r}{V} = Q$

$\Rightarrow -u\frac{\delta T}{\delta \varsigma} = \alpha(\frac{\delta^2 T}{\delta \varsigma^2} + \frac{\delta^2 T}{\delta y^2} + \frac{\delta^2 T}{\delta z^2}) + Q$ (12)

This is a quasi-steady state problem $(\frac{\delta T}{\delta t} = 0)$ *i.e. we solve independent of time.*

Dividing equation (12) through by α, we get:

$$-\frac{u}{\alpha}\cdot\frac{\delta T}{\delta \varsigma} = \frac{\delta^2 T}{\delta \varsigma^2} + \frac{\delta^2 T}{\delta y^2} + \frac{\delta^2 T}{\delta z^2} + \frac{Q}{\alpha}$$

Let $\frac{1}{\alpha} = 2\lambda$

$\Rightarrow -2\lambda\cdot\frac{u\,\delta T}{\delta \varsigma} = \frac{\delta^2 T}{\delta \varsigma^2} + \frac{\delta^2 T}{\delta y^2} + \frac{\delta^2 T}{\delta z^2} + 2\lambda Q$ (13)

Now,

$T = T_0 + e^{-\lambda u\varsigma}\cdot\phi - 2\lambda u e^{-\lambda u\varsigma}\cdot\frac{\delta\phi}{\delta\varsigma}$ (14)

Where;

T_0 = Initial temperature of plate.

ϕ = Function to be determined.

$\Rightarrow \frac{\delta T}{\delta \varsigma} = -\lambda u e^{-\lambda u\varsigma}\cdot\phi + e^{-\lambda u\varsigma}\cdot\frac{\delta\phi}{\delta\varsigma}$ (15)

Similarly,

$\frac{\delta^2 T}{\delta y^2} = e^{-\lambda u\varsigma}\cdot\frac{\delta^2\phi}{\delta y^2}$ (16)

$\frac{\delta^2 T}{\delta z^2} = e^{-\lambda u\varsigma}\cdot\frac{\delta^2\phi}{\delta z^2}$ (17)

Putting all these derivations in (15), we have

$$-2\lambda u(-\lambda u e^{-\lambda u\varsigma}\cdot\phi + e^{-\lambda u\varsigma}\cdot\frac{\delta\phi}{\delta\varsigma}) = (\lambda^2 u^2 e^{-\lambda u\varsigma}\cdot\phi - 2\lambda u e^{-\lambda u\varsigma}\cdot\frac{\delta\phi}{\delta\varsigma} + e^{-\lambda u\varsigma}\cdot\frac{\delta^2\phi}{\delta\varsigma^2}) + (e^{-\lambda u\varsigma}\cdot\frac{\delta^2\phi}{\delta y^2}) + (e^{-\lambda u\varsigma}\cdot\frac{\delta^2\phi}{\delta z^2}) + 2\lambda Q$$

Dividing both sides by $e^{-\lambda u\varsigma}$, we have

$$-2\lambda u(-\lambda u\phi + \frac{\delta\phi}{\delta\varsigma}) = (\lambda^2 u^2\phi - 2\lambda u\cdot\frac{\delta\phi}{\delta\varsigma} + \frac{\delta^2\phi}{\delta\varsigma^2}) + \frac{\delta^2\phi}{\delta y^2} + \frac{\delta^2\phi}{\delta z^2} + 2\lambda Q$$

$\Rightarrow \frac{\delta^2\phi}{\delta\varsigma^2} + \frac{\delta^2\phi}{\delta y^2} + \frac{\delta^2\phi}{\delta z^2} - (\lambda^2 u^2)\phi + 2\lambda Q = 0$ (16)

Equation (12) is a convenient form of the equation for the heat flow in the case of the quasi-steady state of welding.

B. Analytical Solution

Three different types of analytical solutions are typically feasible in welding; one of the reasons welding does not allow for the possibility of having a large number of analytical solutions is due to the nature of the problem, which includes a moving heat source that can have a complicated distribution of

Adedeji. A. Kasali, Zokoro. S. Peter, and Adedeji. T. Emmanuella, "Development of a Thermal Model for the Prediction of Temperature Distribution at Arc Welding Surface," International Research Journal of Advanced Engineering and Science, Volume 8, Issue 2, pp. 165-171, 2023.

International Research Journal of Advanced Engineering and Science
ISSN (Online): 2455-9024

heat and boundary conditions that could include radiation and conduction as well as different conditions on different walls [5].

The three main categories of solutions that are available are listed here; error function based - Rosenthal solutions, and integrals of functions that are listed as we see in class. As a result, unlike the problem, for example, as a heat exchanger or pins, welding is a situation where the analytical solutions are very limited [5].

In this work, Rosenthal's solutions have been considered because the assumptions on which the solutions are based are very similar to the assumptions of the model developed. The assumptions that go behind the solutions of Rosenthal are

1. Heat flow is steady state;
2. The heat source is a point;
3. Heat losses from the surface are neglected;
4. Convection in the weld pool is neglected;
5. Thermal properties are constant;
6. The latent heat of fusion is neglected.

The analytical solution of temperature distribution Rosenthal's 3D equation in a semi-infinite workpiece is given below [15].

$$T = T_0 + \frac{Q}{2\pi kR} exp(\frac{-u(R-x)}{2\alpha}) \quad (17)$$

Where R = Radial distance from the origin;

$$R = \sqrt{(x-x_0)^2 + (y-y_0)^2 + (z-z_0)^2} \quad (18)$$

Q = amount of heat that is transferred to the material;
k = thermal conductivity;
u = Velocity of the torch;
α = Thermal diffusivity.

C. Finite Element Analysis

The analytical solution of temperature distribution Rosenthal's 3D equation in a semi-infinite workpiece is based on a number of assumptions that do not truly express the simulation of a real-life welding process and its results are not sufficient to accurately predict the temperature distribution of an actual welding process; hence, the need to carry out Finite Element Analysis (FEA).[15]

According to Wikipedia, FEA eliminates the assumption of non-constant material properties and allows using non-axisymmetric, three-dimensional heat sources such as ellipsoidal and double ellipsoidal distributions. [11][12]

Consequently, instead of carrying out the finite element analysis using a point heat source, the double ellipsoidal heat source distribution presented by Goldak was used because it is intended to be flexible and to be used to analyze deep or shallow welds and asymmetric geometry. The Goldak model has been shown to agree well with experimental results on thick section submerged arc weld (SAW) on steel plate, partial penetration electron beam weld (EBW) on steel plate, and gas tungsten arc weld (GTAW) on a thin austenitic stainless steel plate. [12]

D. Abaqus Simulation

The procedure for carrying out a welding simulation using ABAQUS software is described as follows:

Step 1: Model Creation

A new standard/explicit model was created to simulate the arc welding process.

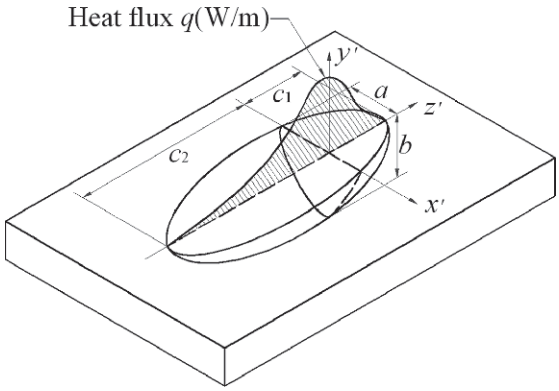

Fig. 2. Goldak's double ellipsoid heat source model. [13]

Step 2: Edit model attributes

The absolute temperature and Stefan Boltzmann constant were specified for the model to accurately represent the thermal behavior of the system being modeled.

Step 3: Part Module

A part instance was created with specified dimensions and saved for use in subsequent modules.

Step 4: Material Properties

Several thermal properties of the material, including density, conductivity, specific heat capacity, latent heat, Young's modulus, strain, yield stress, Poisson's ratio, and expansion coefficient, were considered. The table below shows a material property table for Steel SUS 304 used in carrying out this work.

TABLE I. Thermal, Physical and Mechanical Properties of SUS304.

Temperature (°C)	Specific heat (J/g °C)	Conductivity (J/mm °C s)	Density (g/mm^3)	Yield stress (MPa)	Thermal expansion coefficient (°C^{-1})	Young's modulus (GPa)	Poisson's ratio
0.0000	0.462	0.0146	0.790	265.00	1.70e−5	198.50	0.294
100.00	0.496	0.0151	0.788	218.00	1.74.e−5	193.00	0.295
200.00	0.512	0.0161	0.783	186.00	1.80e−5	185.00	0.301
300.00	0.525	0.0179	0.779	170.00	1.86e−5	176.00	0.310
400.00	0.540	0.0180	0.775	155.00	1.91e−5	167.00	0.318
600.00	0.577	0.0208	0.766	149.00	1.96e−5	159.00	0.326
800.00	0.604	0.0239	0.756	91.00	2.02e−5	151.00	0.333
1200.0	0.676	0.0322	0.737	25.000	2.07e−5	60.00	0.339
1300.0	0.692	0.0337	0.732	21.000	2.11e−5	20.000	0.342
1500.0	0.700	0.120	0.732	10.00	2.16e−5	10.000	0.388

Source: Deng and Murakawa [14]

Step 5: Assembly Module

An instance was created and translated to the center of the part to specify the welding path. The path was partitioned into three sections using datum points and the cutting plane tool.

Step 6: Step Module

Two steps were created to represent the welding and cooling processes. Both steps were defined as Coupled-Displacement types.

Step 7: Interaction Module

Three interactions were created to model the contact between the weld metal and inert gas and air, the contact between the top surface of the weld metal and inert gas and air, and the contact between the whole weld metal and welding radiations.

Step 8: Mesh Module

The global seeds were edited, sizing controls were specified, and the part instance meshed using the specified settings.

Finally, a Python script was used to apply the load to the meshed model and carry out the welding simulation.

Adedeji. A. Kasali, Zokoro. S. Peter, and Adedeji. T. Emmanuella, "Development of a Thermal Model for the Prediction of Temperature Distribution at Arc Welding Surface," International Research Journal of Advanced Engineering and Science, Volume 8, Issue 2, pp. 165-171, 2023.

International Research Journal of Advanced Engineering and Science
ISSN (Online): 2455-9024

III. Results And Discussion

The results of the thermal analysis of the arc welding process using the ABAQUS software will be presented. The visualization module was used to generate the temperature distribution graph and extract the time-temperature data for further analysis.

The temperature distribution graph provided a visual representation of the temperature profile during the welding process. It showed that as the weld moved in one direction, the front part experienced a gradual increase in temperature due to heating, leading to solidification at the back and gradual cooling. The color bar indicates the distribution of temperature for corresponding isotherms, allowing for the definition of the molten zone and heat-affected zone. This is shown in Fig. 3 and Fig. 4 respectively.

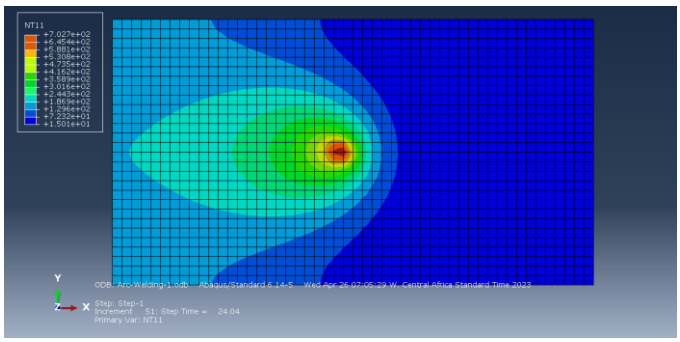

Fig. 3. Nodal temperature heat contour map during welding.

Contour heat maps are a type of graphical representation that shows how a particular property changes in value across a part or structure. In the context of the arc welding simulation, these contour heat maps represent the nodal temperatures of the part instance.

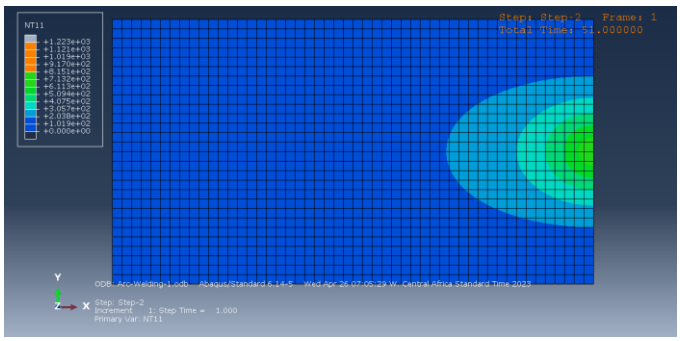

Fig. 4. Nodal temperature heat contour map during cooling.

The nodal temperatures are the temperature values of each finite element node, and they can be visualized using contour heat maps to show the temperature distribution across the part. The contour heat maps are color-coded to represent different temperature ranges, with warmer colors (such as red and yellow) representing higher temperatures, and cooler colors (such as blue and green) representing lower temperatures.

By examining the contour heat maps, the areas of the part that experience higher temperatures during welding were easily identified to be the weld zone. These maps can also be used to optimize the welding process by adjusting parameters such as welding speed, heat input, and material properties to achieve a desired temperature distribution across the part.

A. Nodal Temperature at Two Nodes

To extract the time-temperature data, two (2) nodes were selected at which the temperature data was required. Interpolation was used to obtain data between the selected nodes.

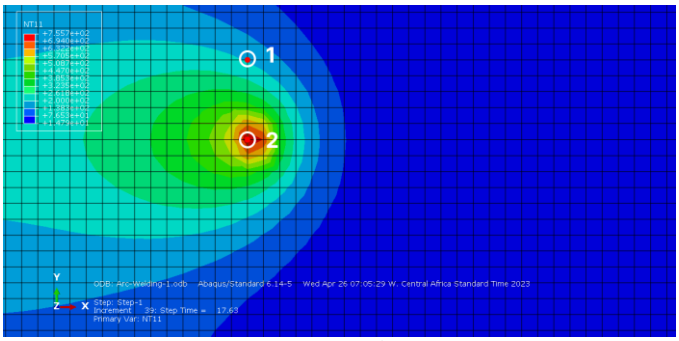

Fig. 5. Two selected nodes for data collection.

The resulting graph showed that the heating cycle rapidly increased the temperature, followed by a cooling cycle. The bump observed in the graph was likely due to a phase transformation between the solidus and liquidus temperatures.

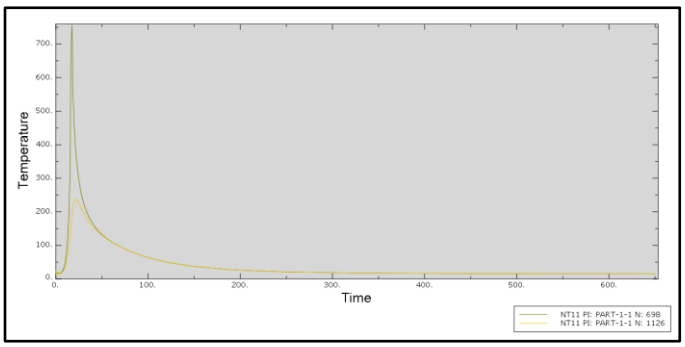

Fig. 6. Graph of Temperature against Time for 2 selected Nodes.

The temperature distribution graph (Fig. 6) displays the temperature changes over time for each node in the model. This graph is essential for understanding the heating and cooling behavior of the part during the welding process.

The graph can be divided into three distinct phases based on the temperature changes observed. The first phase is the preheated phase where the temperature is stable until heat is applied and it starts to rise to the welding temperature. The second phase is the heated phase which starts with a sharp rise in temperature to the welding temperature. Finally, the cooling phase begins as the welding process ends, and the temperature starts to drop gradually until it reaches the ambient temperature. It is important to note that the temperature distribution and the three phases vary based on the location of the node in the part instance.

B. Thermal History

To extract the thermal history data across paths, the nodal paths were selected and grouped under two sets named “Path-

Adedeji. A. Kasali, Zokoro. S. Peter, and Adedeji. T. Emmanuella, “Development of a Thermal Model for the Prediction of Temperature Distribution at Arc Welding Surface,” International Research Journal of Advanced Engineering and Science, Volume 8, Issue 2, pp. 165-171, 2023.

International Research Journal of Advanced Engineering and Science
ISSN (Online): 2455-9024

1" and "Path-2" respectively. Path-1 (Fig. 7) was selected across the welding pool while Path-2 (Fig. 8) is perpendicular to the welding path.

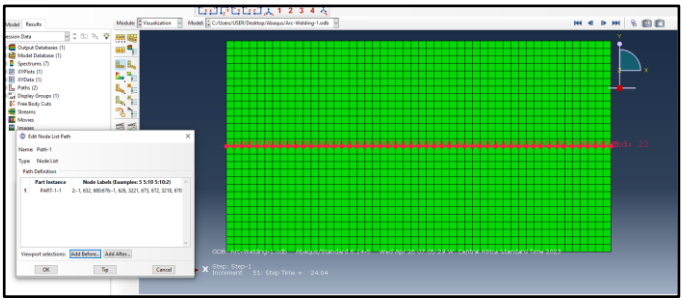

Fig. 7. Nodal path selected across the welding path.

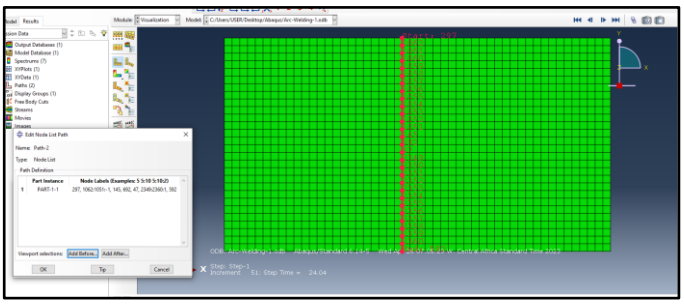

Fig. 8. Nodal path selected perpendicular to the welding path.

The resulting graphs for paths are shown below in Fig. 9 and Fig. 10 respectively.

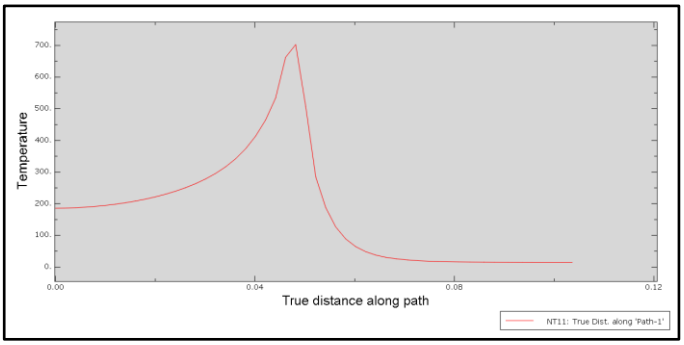

Fig. 9. Graph of Temperature against True Distance along Path-1.

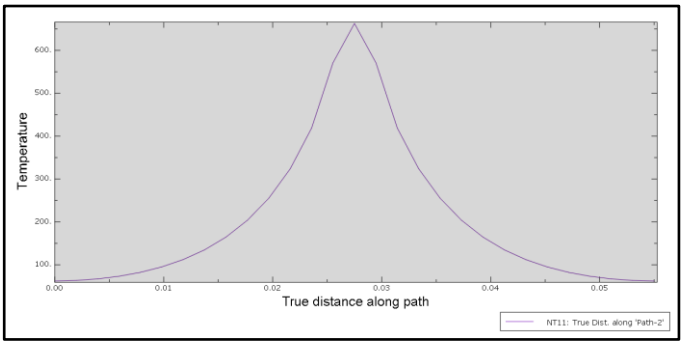

Fig. 10. Graph of Temperature against True Distance along Path-2.

Fig. 9 and Fig. 10 display the thermal history of the weld pool and a perpendicular path, respectively. The temperature profiles are shown as schematics, with temperature on the y-axis and time on the x-axis. During the heating process, the temperature continuously and smoothly increases to a maximum value, as seen in both figures. Once the heat source is turned off, the cooling cycle begins, and the cooling rates are observed to be different from the heating rates.

The FE model allowed the prediction of the temperature distribution not only at individual nodes but also along any path on the part instance, providing valuable insights into the heat-affected zone and potential deformation during welding.

C. *Results Of Stress Analysis*

Furthermore, stress values can also be analyzed and displayed in the form of contour heat maps and depicted on a graph. This enables us to identify areas of the part that are subjected to high levels of stress during welding and evaluate the potential for failure or deformation under such conditions. Some of the charts are shown below with their respective graphs.

Von Mises Stress

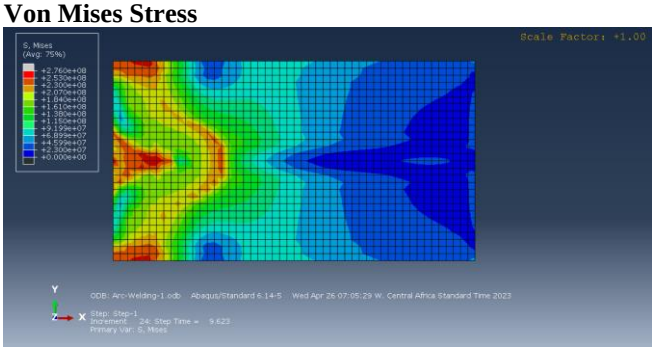

Fig. 11. Heat contour map showing the distribution of Von Mises stresses.

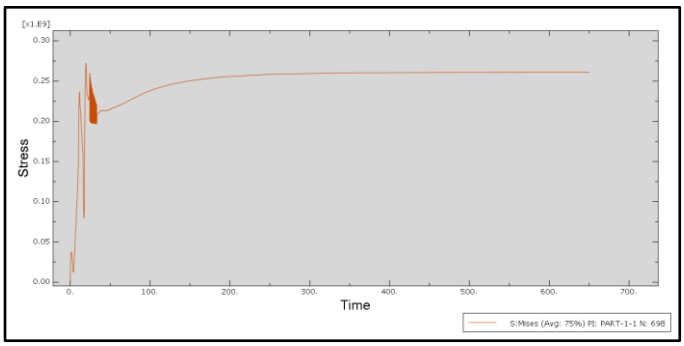

Fig. 12. Graph of Von Mises stresses against time.

Maximum Principal Stress

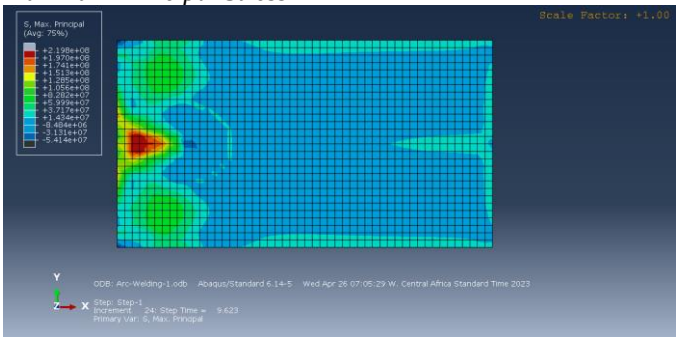

Fig. 13. Heat contour map showing the distribution of Maximum Principal stresses

Adedeji. A. Kasali, Zokoro. S. Peter, and Adedeji. T. Emmanuella, "Development of a Thermal Model for the Prediction of Temperature Distribution at Arc Welding Surface," International Research Journal of Advanced Engineering and Science, Volume 8, Issue 2, pp. 165-171, 2023.

International Research Journal of Advanced Engineering and Science
ISSN (Online): 2455-9024

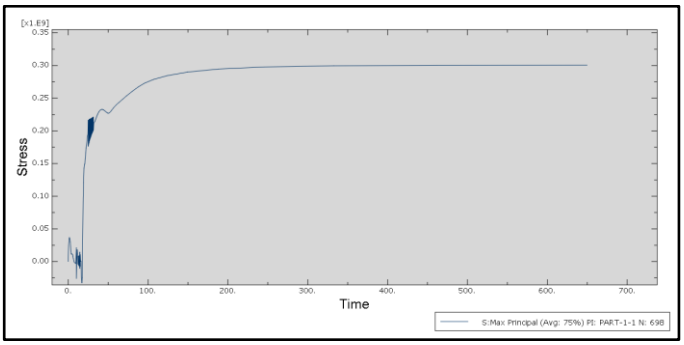

Fig. 14. Graph of Maximum Principal stresses against time.

Minimum Principal Stress

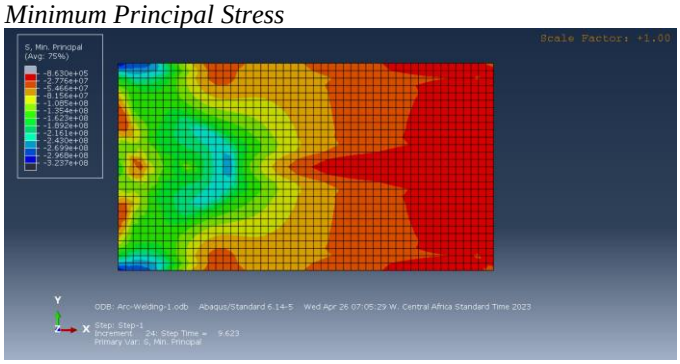

Fig. 15. Heat contour map of the distribution of Minimum Principal Stress.

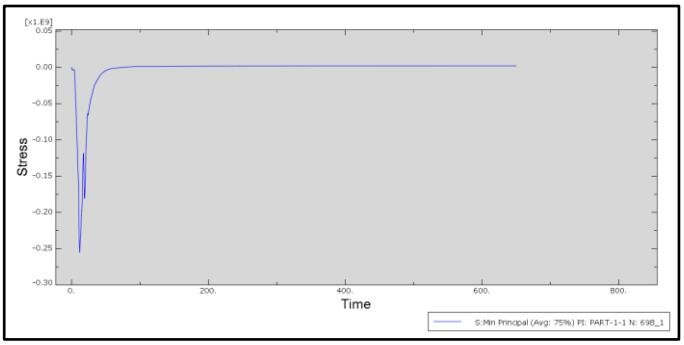

Fig. 16. Graph of Minimum Principal Stress against Time.

Stresses in the local 1 direction (S11)

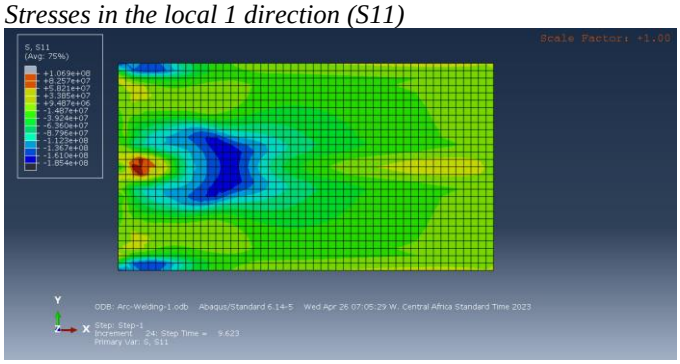

Fig. 17. Heat contour map showing the distribution of S11 stresses.

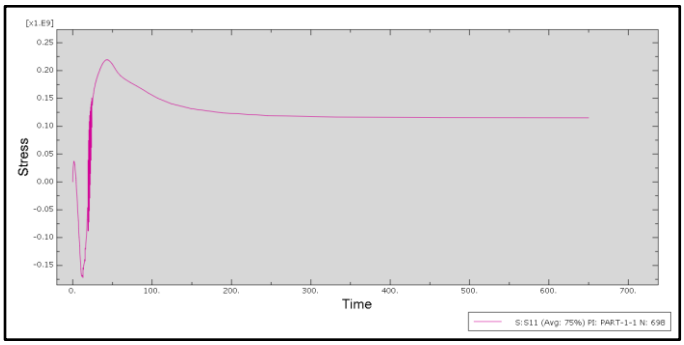

Fig. 18. Graph of S11 stresses against time.

Stresses in the local 2 direction (S22)

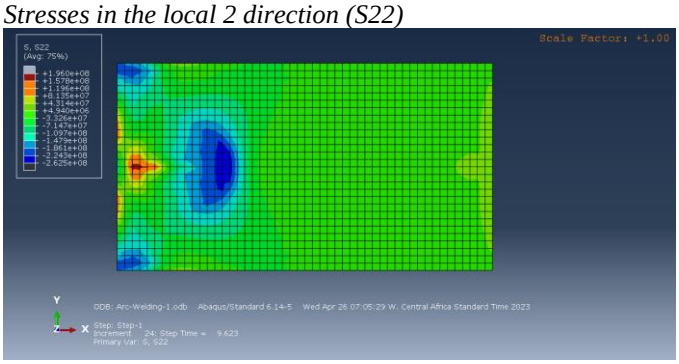

Fig. 19. Heat contour map showing the distribution of S22 stresses.

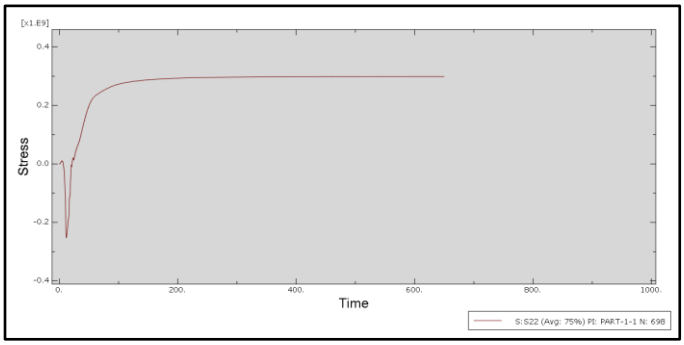

Fig. 20. Graph of S22 stresses against time.

By simulating the welding process, a deeper understanding of the mechanical behavior of the part was gained and this knowledge can be used to optimize them for improved performance and reliability.

IV. CONCLUSION

In conclusion, this study aimed to develop a thermal model in the Arc welding process for the prediction of temperature distribution at the welding surface. The primary objective of the study has been achieved with the successful development of a 3-D FE thermal model using the ABAQUS software, which was used to model the arc welding process. The simulation results, which include graphs and contour heat maps, provide a better understanding of the temperature distribution at the welding surface.

Through a review of existing literature and the development of a mathematical model, this study contributes to the advancement of knowledge in the field of thermal modeling in arc welding. The findings of this study have practical

Adedeji. A. Kasali, Zokoro. S. Peter, and Adedeji. T. Emmanuella, "Development of a Thermal Model for the Prediction of Temperature Distribution at Arc Welding Surface," International Research Journal of Advanced Engineering and Science, Volume 8, Issue 2, pp. 165-171, 2023.

applications in industries that use welding as a means of joining metals.

However, it is essential to note that there is still much work to be done to improve the accuracy of the model. Future work should focus on the optimization of the mesh element size and proper load application. It is also recommended that credible sources of information be used for the inputs to the FEA model to ensure accurate results.

In summary, this study provides a significant contribution to the field of thermal modeling in arc welding, and the findings can be used to improve welding processes in various industries.

REFERENCES

[1] American Welding Society. (2013). Welding Handbook: Welding Processes, Volume 2 (9th ed.). Miami, FL: American Welding Society.
[2] Li, J., Chen, L., Li, Y., & Gao, M. (2016). Modeling and simulation of temperature field during laser beam welding of dissimilar materials. Journal of Materials Processing Technology, 234, 13-22.
[3] Xu, G., He, Y., & Wang, G. (2018). Numerical simulation of temperature field during arc welding using finite element method. International Journal of Advanced Manufacturing Technology, 94(5-8), 1815-1823.
[4] Zhang, J., Dong, S., Zhang, X., & Hu, S. J. (2019). Development of a three-dimensional thermal model for gas tungsten arc welding and gas metal arc welding. Journal of Manufacturing Science and Engineering, 141(4), 041011.
[5] IIT Roorkee July 2018. (2019, June 22). Temperature Distribution in Welding [Video]. YouTube. Temperature Distribution in Welding
[6] Analysis and Modeling of Welding. (2016, January 29). Analytical Solutions to Weld Thermal Field [Video]. YouTube. Analytical Solutions to Weld Thermal Field
[7] Handbook of Mathematical Functions - M. Abramowitz & I.A. Stegun, National Bureau of Standards, Washington DC (1964)
[8] Conduction of heat in solids - H.S. Carslaw and J.C. Jaeger, 2nd Edition, Oxford University Press, London (1959)
[9] Transport Phenomena and Materials Processing - Sindo Kou, John Wiley & Sons, (1996)
[10] Rosenthal, D. (1946) The Theory of Moving Sources of Heat and Its Application to Metal Treatments. Transactions ASME, 43, 849-866
[11] Moving heat source model for thin plates. (2023, February 28). In Wikipedia. Moving heat source model for thin plates - Wikipedia
[12] Goldak, J.A., Chakravarti, A.P., & Bibby, M. (1984). A new finite element model for welding heat sources. Metallurgical Transactions B, 15, 299-305.
[13] M. Hashemzadeh; et al. (2013). "Comparison Between Different Heat Sources Types in Thin-Plate Welding Simulation". Developments in Maritime Transportation and Exploitation of Sea Resources. London, UK: Francis & Taylor Group.
[14] Deng, D., & Murakawa, H. (2006). Numerical simulation of temperature field and residual stress in multi-pass welds in stainless steel pipe and comparison with experimental measurements. Computational Materials Science, 37(3), 269–277. https://doi.org/10.1016/j.commatsci.2005.07.007
[15] Adedeji. A. Kasali, Nurudeen. A. Raji, Fadipe.O. Lukman, Aderibigbe.O. Michael. (2020). “Simulation and Investigations of the Effect of Cutting Parameters on Chip Formation of Aluminium Alloy 6061-T6 ” International Journal of Scientific & Engineering Research Volume 11, Issue 3, ISSN 2229-5518, Pp 1562-1577.